

# THE EARLY EARLY TYPE: DISCOVERY OF A PASSIVE GALAXY AT $z_{\text{spec}} \sim 3$

R. GOBAT<sup>1</sup>, V. STRAZZULLO<sup>1</sup>, E. DADDI<sup>1</sup>, M. ONODERA<sup>2</sup>, A. RENZINI<sup>3</sup>, M. BÉTHERMIN<sup>1</sup>, M. DICKINSON<sup>4</sup>, M. CAROLLO<sup>2</sup>,  
A. CIMATTI<sup>5</sup>

*Draft version July 11, 2018*

## ABSTRACT

We present the discovery of a massive, quiescent galaxy at  $z = 2.99$ . We have obtained a *HST*/WFC3 spectrum of this object and measured its redshift from the detection of a deep 4000 Å break consistent with an old population and a high metallicity. By stellar population modeling of both its grism spectrum and broad-band photometry, we derive an age of  $\sim 0.7$  Gyr, implying a formation redshift of  $z > 4$ , and a mass  $> 10^{11} M_{\odot}$ . Although this passive galaxy is the most distant confirmed so far, we find that it is slightly less compact than other  $z > 2$  early-types of similar mass, being overall more analogous to those  $z \sim 1.6$  field early-type galaxies. The discovery of this object shows that early-type galaxies are detectable to at least  $z = 3$  and suggests that the diversity of structural properties found in  $z = 1.4 - 2$  ellipticals to earlier epochs could have its origin in a variety of formation histories among their progenitors.

*Subject headings:* galaxies: evolution—galaxies: formation—galaxies: high-redshift

## 1. INTRODUCTION

In the nearby Universe, most stars reside in massive, passively evolving spheroidal systems, either spiral bulges or elliptical galaxies (Baldry et al. 2004). Early-type galaxies (ETG), such as ellipticals and lenticulars, are often the most massive galaxies in their surrounding environment and ETGs include the dominant stellar component in clusters of galaxies. As far as they can be found in significant numbers, massive ETGs exhibit very homogeneous spectrophotometric properties, requiring that their stellar content formed rapidly at relatively high redshifts and evolved passively for most of the cosmic time. In particular, studies of the core ETG population in galaxy clusters suggest that the quenching of their star formation (SF) was already underway by  $z \sim 3$ .

The precursors of  $z \lesssim 1$  massive elliptical galaxies can arguably be found in some high-redshift submillimeter-selected galaxies, whose extreme star-formation rates (SFRs, in excess of  $1000 M_{\odot} \text{ yr}^{-1}$ ; Daddi et al. 2009; Michałowski et al. 2010) imply that they should exhaust their gas reservoirs on short time scales (e.g., Carilli et al. 2010) and thus offer a striking example of rapid, unsustainable growth at early epochs. The spheroidal morphology of ETGs might then be either the consequence of merging events, triggering the starburst or happening after the quenching of SF, or dynamical instabilities internal to the galaxies (e.g., Martig et al. 2009; Bournaud, Elmegreen & Martig 2009). This latter process may actually be the dominant one, given that

the vast majority ( $\sim 86\%$ ) of ETGs are fast rotators (Emsellem et al. 2011).

One would therefore expect to find quenched, massive ETGs already at  $z \sim 2 - 3$  and indeed passively evolving galaxies (PEGs; generally color selected as passive and not necessarily morphologically early-type) have been spectroscopically confirmed up to  $z \sim 2.5$  (van Dokkum et al. 2008). Most of these early passive systems appear to be up to a factor  $\sim 10$  denser than their modern counterparts (e.g., Daddi et al. 2005; Cimatti et al. 2008; van Dokkum et al. 2008). However, the search for high-redshift ETGs is hampered not only by the expected rarity of such objects, but also by the intrinsic difficulty in reliably detecting them and measuring their redshifts. The most distinctive spectral feature of ETGs, the pronounced metal break at 4000 Å is redshifted to the near-infrared at  $z > 1$  and detection, let alone characterization, of  $z \sim 2$  ETGs requires good continuum signal to noise (S/N) only achievable with extremely long exposures from the ground. Consequently, the sample of confirmed  $z \gtrsim 2$  ETGs is still small, and its high-redshift tail, i.e., the earliest epoch at which passive galaxies can be found, poorly constrained.

Here we present the serendipitous discovery of the most distant spectroscopic ETG so far identified, i.e., a massive and passive galaxy at  $z \sim 3$ . Throughout the Letter, we assume a  $\Lambda$ CDM cosmology with  $H = 70 \text{ km s}^{-1} \text{ Mpc}^{-1}$ ,  $\Omega_m = 0.27$  and  $\Lambda = 0.73$ . Magnitudes are given in the AB photometric system.

## 2. OBSERVATIONS

This object (hereafter RS-235) was discovered in deep *HST*/WFC3 observations of the  $z \sim 2$  cluster Cl J1449+0856 (Gobat et al. 2011) at 14:49:16.5, +8:55:34.7, about  $56''$  from the center of the structure. These data cover a  $6.4 \text{ arcmin}^2$  field centered on Cl J1449+0856 and consist of 2 orbits of imaging with the *F140W* filter and 16 orbits of spectroscopy with

<sup>1</sup> Laboratoire AIM-Paris-Saclay, CEA/DSM-CNRS-Université Paris Diderot, Irfu/Service d'Astrophysique, CEA Saclay, Orme des Merisiers, F-91191 Gif sur Yvette, France

<sup>2</sup> Institute for Astronomy, ETH Zürich, Wolfgang-Pauli-strasse 27, 8093 Zürich, Switzerland

<sup>3</sup> INAF - Osservatorio Astronomico di Padova, Vicolo dell'Osservatorio 5, I-35122 Padova, Italy

<sup>4</sup> National Optical Astronomy Observatory, P.O. Box 26732, Tucson, AZ 85726, USA

<sup>5</sup> Dipartimento di Astronomia, Università di Bologna, Via Ranzani 1, I-40127 Bologna, Italy

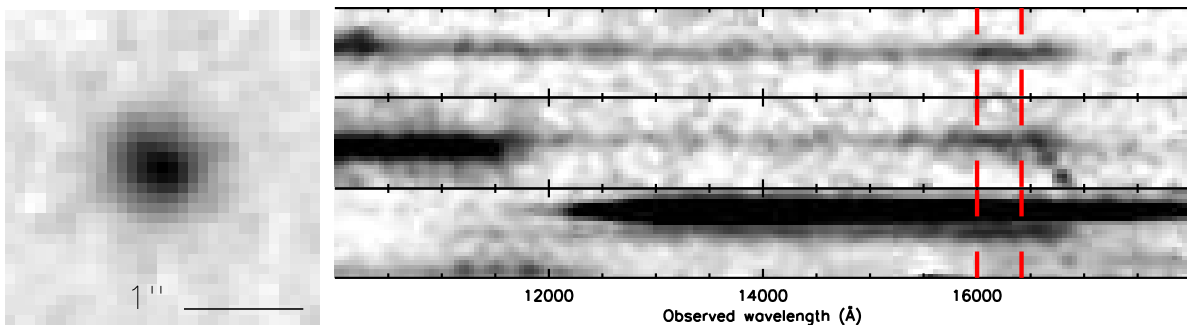


**Figure 1.** Left:  $2''.6 \times 2''.6$  *HST*/WFC3 *F140W* image of RS-235. The image is  $2''.6 \times 2''.6$  wide, with a pixel size of  $0''.06$ . Right: two-dimensional spectra of RS-235 in each of the three orientations, between 1 and  $1.8 \mu\text{m}$ , smoothed with a 2 pixel bin. The bottom spectrum suffers from slight contamination between  $1.25$  and  $1.5 \mu\text{m}$  from the tail of a bright, parallel second order trace and the two others have overlapping traces below  $1.2 \mu\text{m}$ . Each pixel is  $46.5 \text{ \AA}$  ( $\sim 11.7 \text{ \AA}$  in rest-frame) wide in the dispersion direction and  $\sim 0''.13$  in the spatial (vertical) direction. The red lines bracketing the spectrum show the position of the  $4000 \text{ \AA}$  break and  $\text{H}_\delta$ , respectively.

the G141 grism, in three different orientations. The individual frames were sky-subtracted and reduced using the best available calibration files. Standard procedures were applied: the WFC3 images were combined with MultiDrizzle and grism spectra for each orientation extracted with the aXe pipeline (Kümmel et al. 2009).<sup>6</sup> The *F140W* image of RS-235, as well as the two-dimensional spectra in the three orientations, is shown in Figure 1. Trace contamination was modeled using the *F140W* deep image ( $m_{140} = 26.5$  AB at  $5\sigma$  in a  $1''$  aperture) and the multiwavelength dataset already available for this field. This extensive set of ground-based observations was first described in Gobat et al. (2011) and has recently been extended with deep *U* and *V*-band VLT/FORS2 imaging and deeper  $3.5\text{--}4.5 \mu\text{m}$  *Spitzer*/IRAC imaging, in addition to the *HST*/WFC3 data. At longer wavelengths,  $24 \mu\text{m}$  *Spitzer*/MIPS data were already available and *Herschel*/PACS 100 and  $160 \mu\text{m}$  observations have recently been obtained to expand the dataset (the maps reach a  $5\sigma$  depth of  $1.5$  and  $2.8$  mJy respectively and will be described in a forthcoming paper). We have used this new multiwavelength (*U*-band to IRAC) catalog to compute photometric redshifts for all objects in the *HST*/WFC3 field with EAZY using the standard set of templates (Brammer et al. 2008, 2011).

RS-235 stood out in this dataset as having a 2D spectrum with a pronounced break at  $\sim 1.6 \mu\text{m}$ , a well-constrained photometric redshift of  $z \sim 3$  and rest-frame *UVJ* colors consistent with an old stellar population (Wuyts et al. 2007). Furthermore, RS-235 is not seen at  $24$ ,  $100$  or  $160 \mu\text{m}$  although, due to its redshift and the depth of the maps, this non-detection only provides very loose constraints on its SFR, with an upper limit of  $\text{SFR} < 400 M_\odot \text{ yr}^{-1}$  assuming recent templates from Magdis et al. (2012).

To ensure that the spectrum of RS-235 is free of contamination so that its continuum shape can be measured reliably, we performed, for each of the three WFC3 orientations, two different extractions from the cutout produced by aXe. We first used a 3 pixel aperture, roughly corresponding to the FWHM of the object, and linearly fitted the observed spectrum with the combined contam-

ination and trace models. We compared the resulting one-dimensional spectrum with that obtained from fitting each cross-dispersion column of the cutout with profiles derived, for each trace, from the profile of the corresponding object in the *F140W* image. The decontaminated spectra were then stacked to produce a single high S/N ( $\sim 11 \text{ pixel}^{-1}$  at  $1.6 \mu\text{m}$ ) spectrum and converted to flux units. We note that, while the first orientation suffers from moderate contamination between  $1.25$  and  $1.5 \mu\text{m}$  (from the tail of a bright non overlapping trace) and the other two below  $1.25 \mu\text{m}$  (from overlapping traces), the region redward of  $1.5 \mu\text{m}$  where the break is seen is entirely free from contamination in all three cases. The sampling of the spectrum is  $46.5 \text{ \AA}$  with the G141 grism and its FWHM resolution  $126 \text{ \AA}$ , as grism spectra are convolved with the brightness profile of the dispersed sources. In this case, the profile is sufficiently circular ( $b/a \sim 0.8$ ) that it was not necessary to optimize the orientation of the pseudo-slit during extraction.

### 3. ANALYSIS

As shown in Figure 2, the stacked spectrum shows two distinct spectral features: the break at  $1.6 \mu\text{m}$  and an absorption feature ( $\text{H}_\delta$ ) at  $1.636 \mu\text{m}$ . Their position suggests a redshift of  $z \simeq 3$ , which was measured by comparison with templates (see below), yielding  $z = 2.993 \pm 0.015$ . As its spectrophotometry precludes dusty SF solutions (see below), this makes RS-235 the most distant PEG confirmed so far.

#### 3.1. Spectrophotometric modeling

To estimate the stellar mass and characterize the stellar population of the galaxy, we compared both the combined 15-band spectral energy distribution (SED) and high S/N part ( $1.4\text{--}1.65 \mu\text{m}$ ) of the stacked grism spectrum to a range of stellar population models. These were built using high resolution Bruzual & Charlot (2003) and Maraston (2005) (hereafter BC03 and M05) single stellar population templates, assuming  $Z = (1 - 2)Z_\odot$  (see below), a Salpeter (1955) initial mass function (IMF). We considered two different sets of star formation histories (SFH): a delayed, exponentially declining SFH with characteristic time scale  $\tau$  between 1 Myr and 2 Gyr and ages from 100 Myr to the age of the Universe at  $z = 3$ , and a rising exponential SFH of the form  $\text{SFR}(t) = M_0 \times A \times e^{At}$ , starting at  $z_0 = 10$ . The first one can be considered a versatile, albeit simplistic, “generic”

<sup>6</sup> See e.g., [http://www.stsci.edu/hst/wfc3/analysis/grism\\_obs/cookbook.html](http://www.stsci.edu/hst/wfc3/analysis/grism_obs/cookbook.html)

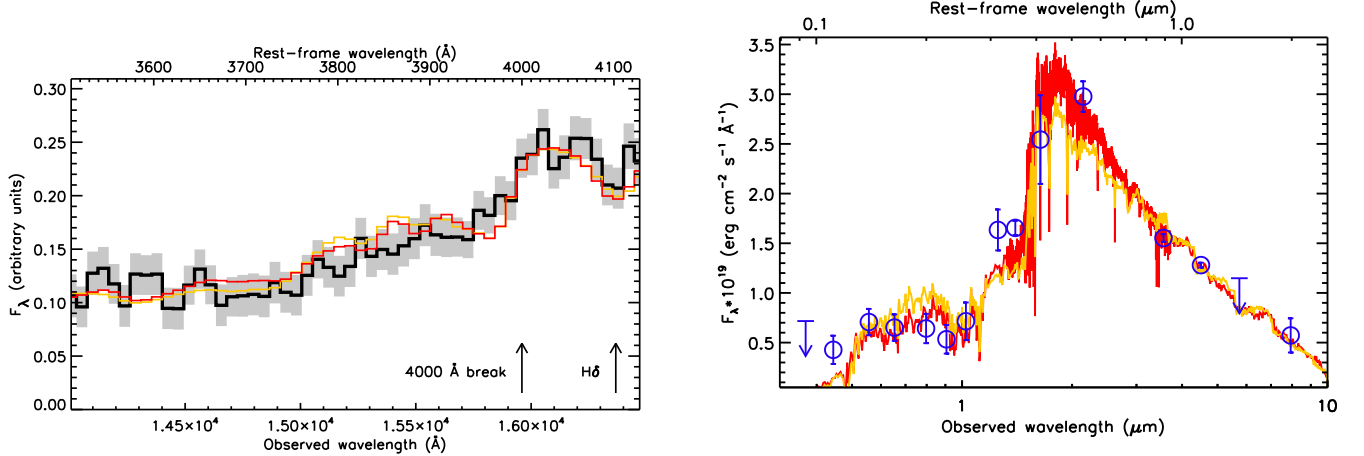


**Figure 2.** Left: *HST*/WFC3 G141 spectrum of RS-235 (black) and associated errors (gray), after subtraction of the contamination and stacking of the three orientations, compared with the best solution to the combined fit to the SED and spectrum (BC03 in red, M05 in orange). Right: 15-band (*UBVRIZYJm<sub>140</sub>HK<sub>s</sub>*+IRAC) SED of RS-235 (blue) and associated errors ( $3\sigma$  upper limits are shown as arrows) with the same BC03 and M05 best solutions (red and orange, respectively) to the combined fit.

SFH, while the second scenario is meant to put lower limits to the average SFR and formation time scales required to produce a galaxy such as RS-235. It is appropriate for a galaxy on the “main sequence” (MS) of star forming galaxies and relies on the apparent weak evolution of the specific SFR (sSFR) at  $z \gtrsim 2.5$  (e.g., Magdis et al. 2010; González et al. 2010; Karim et al. 2011), which indeed implies an exponential growth. Its two parameters are the initial mass  $M_0$  of the galaxy at the beginning of MS evolution, and the parameter  $A$  setting the time scale and determined by the normalization of the SFR- $M^*$  relation at  $z \sim 2.5$ . A shallower slope of the SFR- $M^*$  relation, e.g., a slope  $\sim 0.8$  found by Rodighiero et al. (2011), would imply a power-law SFH with  $\text{SFR}(t) \propto t^4$ , whereas the exponential form has a simpler dependence on  $M_0$ . We allowed values up to 0.7 dex below and above the MS.

In both cases we allowed for a SF cut-off at an arbitrary time to be determined by the best fit procedure, with an option for a secondary burst after the initial quenching contributing up to 50% of the final mass. This addition is motivated by the detection of the galaxy in the rest-frame far-UV (the *V* band, as shown in Figure 2) implying the presence of a small amount of massive stars. Note that the detection in *B* is marginal, at  $\gtrsim 3\sigma$ , and might be due to contamination from a nearby source. Dust extinction was also added using a Calzetti et al. (2000) extinction law and recombination lines were computed using Gaussian profiles of matching resolution, assuming the SFR-*Hα* calibration of Kennicutt (1998) and standard line ratios (Anders & Fritze-v. Alvensleben 2003). The model spectra were convolved with the filters responses to produce synthetic SEDs, smoothed to the resolution of the grism spectrum using a Gaussian kernel and rebinned to match the observed spectrum. The results of the fit are shown in Figure 2 and in Table 1.

Due to the low resolution of the grism spectrum, the spectral fit is mainly constrained by the shape of the continuum, namely the break at  $\sim 1.6 \mu\text{m}$  and the blueward slope of the spectrum, and the lack of prominent spectral features. Notably, the spectrum

does not show any [OII]3727 emission. We find a mean stellar age of  $t_{SF} = 0.7^{+0.15}_{-0.1}$  Gyr (corresponding to  $z_f > 4$ ), with a last episode of SF contributing less than 10% of the final mass of  $M_* = 1.2^{+0.5}_{-0.2} \times 10^{11} M_\odot$ . For the delayed exponential SFH, the fit yields time scales of  $\leq 200$  Myr. In the exponential SFH case, solutions with sSFR below the fiducial MS value ( $\sim 3 \text{ Gyr}^{-1}$  at  $10^{11} M_\odot$ , using Béthermin et al. (2012)) require apparently unrealistic seed masses of  $> 10^9 M_\odot$  at  $z = 10$  (see e.g., M. Sargent et al., in preparation). In this case, the fit implies doubling time-scales of 220 Myr or less. The amount of extinction compatible with the SED is small,  $E(B - V) < 0.1$ , and the fit accordingly rules out star-forming solutions, yielding a negligible residual SFR of  $0 - 0.5 M_\odot \text{ yr}^{-1}$ . RS-235 thus appears to have sSFR of less than  $5 \times 10^{-3} \text{ Gyr}^{-1}$ , at least 2.7 dex below the MS of star forming galaxies at  $z \sim 3$ . Interestingly, models based on Maraston (2005) templates provide a less good fit to the rest-frame optical-NIR SED, underpredicting the flux in the observed *K<sub>s</sub>* band (rest-frame 5000–6000 Å). As RS-235 is still a young stellar population, this could be due to, e.g., the effect of thermally pulsing-asymptotic giant branch stars in the M05 models (which would produce a shallower Rayleigh-Jeans slope) or the presence of convective overshooting in the stellar tracks used by the BC03 models (Maraston et al. 2006).

### 3.1.1. Metallicity

Interestingly, solar metallicity models are rejected at  $> 3\sigma$  by the stellar population modeling. Quantifying the strength of the 4000 Å break using the  $D_N4000$  index (Balogh et al. 1999), we find  $D_N4000 = 1.62 \pm 0.08$  (where uncertainties were estimated through Monte Carlo simulations based on the error spectrum). As shown in Figure 3, this value is comparable to that of a maximally old ( $z_f = 10$  SSP)  $Z = Z_\odot$  stellar population, implying that this is a lower limit to the metallicity of RS-235 and suggesting that the strength of the break requires not only a passive stellar population but also a stellar metallicity above the solar value. We note that the significantly

**Table 1**  
Physical and Structural Parameters from Modeling

$z$	$D_{\text{N}4000}$	$\log M_{\star}$ ( $M_{\odot}$ )	$t_0^{\text{a}}$ (Gyr)	$t_{\text{SF}}^{\text{b}}$ (Gyr)	$r_e$ ( $''$ )	$n$
$2.993 \pm 0.015$	$1.62^{+0.09}_{-0.08}$	$11.08^{+0.15}_{-0.12}$	$0.9^{+0.8}_{-0.2}$	$0.7^{+0.15}_{-0.10}$	$0.16^{+0.02}_{-0.02}$	$1.8 \pm 0.3$

<sup>a</sup> Look-back time to the beginning of star formation

<sup>b</sup> SF-weighted age, i.e., look-back time at which the galaxy formed half of its stars

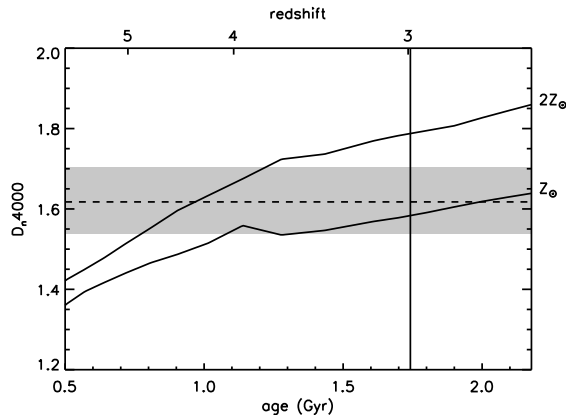


**Figure 3.**  $D_{\text{N}4000}$  index as a function of age and redshift, for unreddened SSPs of solar and twice solar metallicity formed at  $z = 10$ . The dashed horizontal line and gray area show the value of  $D_{\text{N}4000}$ , and associated uncertainty, of RS-235 and the vertical line marks its redshift.

worse resolution of the *HST*/WFC3 G141 spectra, compared to that of the slit spectra of lower redshift objects, on which the  $D_{\text{N}4000}$  index is usually measured, can affect the apparent strength of the break. While this effect depends on the stellar population mix and is most pronounced in the case of SSPs, we find that at our effective resolution the correction is negligible for the best fitting template to the spectrum.

### 3.2. Structural parameters

RS-235 is a resolved object in the *F140W* image, with a FWHM size of  $\sim 2.5$  resolution elements ( $\sim 0''.32$ ). We measured its morphological properties by fitting the surface brightness profile with a Sérsic model (Sérsic 1963) using GALFIT 3 (Peng et al. 2010). We constructed a median point-spread function by combining six unsaturated, high S/N stars in our *HST*/WFC3 field. RS-235 is relatively isolated, with the nearest sources being at least  $2''.3$  away and 1.5 mag fainter. The morphological analysis is therefore stable whether we include the closest neighbors or not. From a series of GALFIT simulations we find that the bias on structural parameters is negligible for a 24 mag object like this galaxy. The scatter on  $r_e$  and  $n$  is about 10% and 20% respectively, which we adopt as the standard error on the parameters. Accordingly, the Sérsic fit yields a circularized effective radius of  $r_e = 0.16 \pm 0''.02$ , or 1.3 kpc at  $z = 2.99$ , and a Sérsic index of  $n = 1.8 \pm 0.3$ . In Figure 4 we compare structural and stellar population parameters of RS-235 with samples of PEGs in the field at  $z \sim 1.6$  (Onodera et al. 2012) and  $z \sim 2.3$  (van Dokkum et al. 2008; Kriek et al. 2009).

We note that we can not *a priori* discount the possibility that RS-235 be lensed by the cluster Cl J1449+0856, as it is relatively close to it, and its observable properties (mass and size) therefore affected. To estimate this effect, we assumed a simple lens model with a single halo of mass  $10^{14} M_{\odot}$  (conservatively twice the X-ray mass, to account for the fact that the structure is likely not entirely virialized) at  $z \sim 2$ , centered on the X-ray emission (see Gobat et al. 2011). Considering both singular isothermal or Navarro, Frenk & White (1996) profiles with  $c \geq 1$ , we derive a magnification of less than 3%, almost a factor 10 lower than the uncertainties on either mass or size and thus negligible. We similarly estimate that the closest projected neighbors of RS-235 do not generate any appreciable lensing effect. On the other hand, we find a magnification of up to 7% for a relatively bright spiral galaxy at  $5''.2$  and  $z_{\text{phot}} = 0.9$ , implying that the stellar mass could be overestimated by this much and the size by  $\sim 3\%$ . Although these factors are lower than the systematic error on either parameter, we added 7% and 3% to the lower uncertainties on the mass and circularized effective radius, respectively, to take the effect of magnification into account.

## 4. DISCUSSION

RS-235 appears to be a quenched, if not entirely passive galaxy at  $z = 2.99$ , the most distant spectroscopically confirmed so far. Its spectrophotometric properties suggest that this galaxy formed the bulk of its stars relatively quickly at  $z \gtrsim 4$  and already has a high metallicity, comparable to that of local ETGs (e.g., Gallazzi et al. 2006). With  $n \sim 1.8$ , it has a flatter profile than the typical passive population at lower redshifts and appears to have not acquired yet a characteristic ETG morphology. As with the vast majority of  $z > 1.5$  PEGs, it is also more compact (2–3 times below the local mass-size relation for ETGs; Shen et al. 2003) than present-day ETGs, although apparently less so than other  $z > 2$  passive galaxies of similar mass and rather well within the variation of  $z \sim 1.6$  galaxies shown in Figure 4. We note that our size measurement was made on a rest-frame near-UV (350 nm) image, as were the measurements by Onodera et al. (2012), while van Dokkum et al. (2008) used rest-frame optical (480 nm) data. Based on the stellar population modeling, we estimate that the flux contribution of young ( $< 500$  Myr) stars increases only by 10%–30% from 480 to 350 nm, thus, this younger component, if present, should not affect much the effective radius measurement. As, additionally, the morphology of high-redshift ETGs has not been observed to vary significantly between the rest-frame near-UV and optical (e.g., Cassata et al. 2012), it is unlikely that the somewhat lower

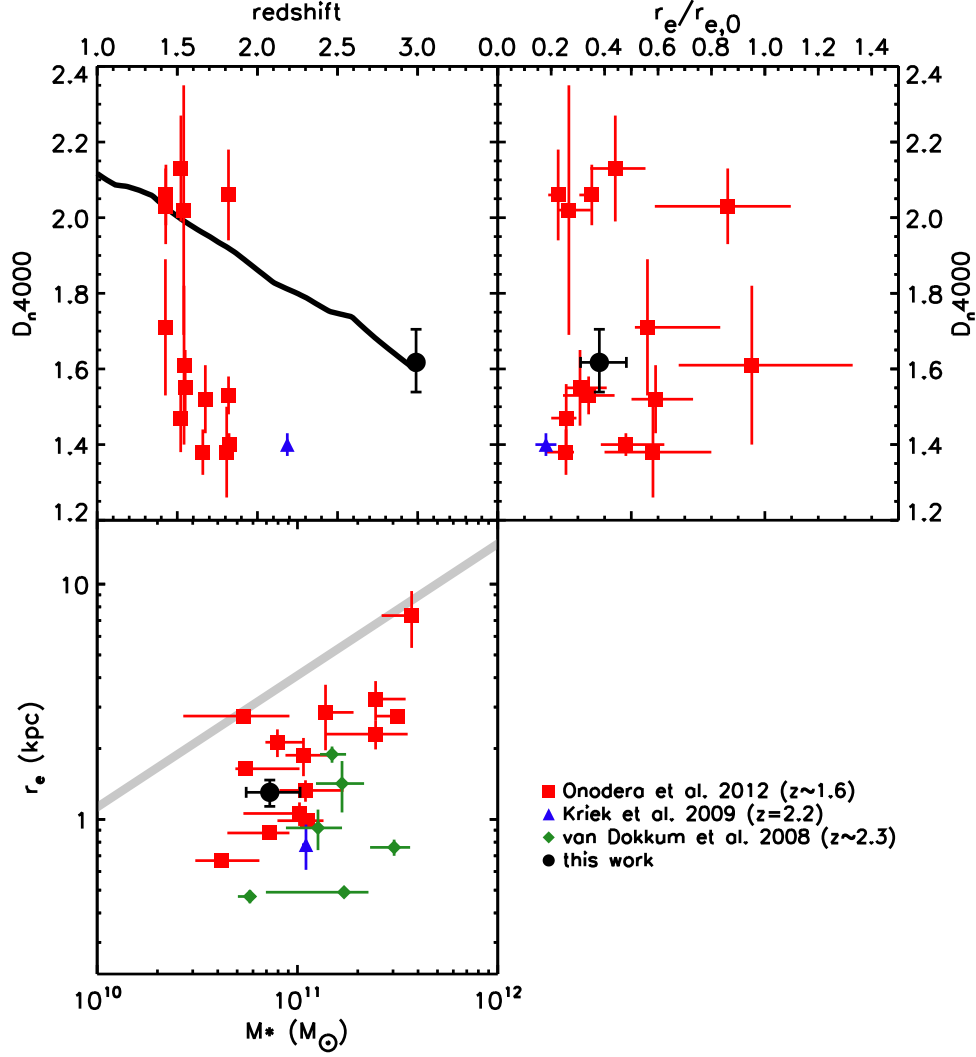


**Figure 4.** Comparison of spectral and structural properties of RS-235 and other high redshift field PEGs (Onodera et al. 2012; Kriek et al. 2009; van Dokkum et al. 2008), excluding objects with disk-like ( $n \lesssim 1$ ) morphology. Top, left:  $D_n4000$  as a function of redshift. The black line shows the evolution of  $D_n4000$  of RS-235, if the galaxy were to evolve passively to lower redshifts. Top, right:  $D_n4000$  vs. the circularized effective radius as a fraction of the value expected from the local mass-morphology relation (Shen et al. 2003). Bottom, left: circularized effective radius as a function of the stellar mass (converted to a Chabrier (2003) IMF), with the local relation shown as a gray line.

surface density of RS-235 compared to the van Dokkum et al. (2008) sample could be due to a positive age gradient. On the other hand, the population of PEGs at  $z = 1.4 - 2$  has been found to be diverse in terms of structural properties with some early-types having a size comparable to that of local ETGs (Saracco et al. 2011; Onodera et al. 2010; Mancini et al. 2010). The existence of a  $z = 3$  passive galaxy, very close to its formation epoch, as extended as the  $z \sim 1.6$  population reinforces this picture and suggests that the diversity of  $z \lesssim 2$  ETGs could reflect not only a spread in assembly histories but also the existence of different formation pathways for these early ETGs.

For example, the compactness of high-redshift ETGs is expected to depend on whether they were produced through gas-rich or gas-poor mergers (e.g., Springel & Hernquist 2005; Bournaud et al. 2011), or through secular gas exhaustion. However, the available data do

not allow us to favor a particular formation scenario, although the relatively low Sérsic index is not indicative of a recent (major) merger. On the other hand, the spectrophotometric fit tends to favor solutions with short doubling time scales and accelerated evolution at high redshift, with respect to our fiducial MS.

Finally, as shown in Figure 4, there are five non-disk PEGs in the Onodera et al. (2012) sample with  $D_n4000$  equal or higher than that of RS-235 at the same epoch, assuming passive evolution of the best fit models. These galaxies are likely to be at least as old as RS-235 and to have been already quenched at  $z \sim 3$ . Their surface density,  $0.08 \pm 0.04 \text{ arcmin}^{-2}$ , is compatible with our single detection in a  $6.4 \text{ arcmin}^2$  field, suggesting that they and RS-235 come from the same early PEG population. It also implies that confirmation of further  $z \sim 3$  PEGs would require relatively few appropriately deep WFC3 pointings and should thus be quite feasible, although the

response of the G141 grism will limit the identification of the 4000 Å break to  $z < 3.1$  until newer instruments, such as NIRSpec on the *James Webb Space Telescope*, become available.

RG, VS, ED and MB were supported by grants ERC-StG UPGAL 240039 and ANR-08-JCJC-0008.

#### REFERENCES

- Anders, P. & Fritze-v. Alvensleben, U. 2003, *A&A*, 401, 1063
- Baldry, I.K., Glazebrook, K., Brinkmann, J., et al. 2004, *ApJ*, 600, 681
- Balogh, M.L., Morris, S.L., Yee, H.K.C., Carlberg, R.G. & Ellingson, E. 1999, *ApJ*, 527, 54
- Béthermin, M., Daddi, E., Magdis, G.E., et al. 2012, *ApJ*, 757, 23
- Bournaud, F., Elmegreen, B.G., Martig, M. 2009, *ApJ*, 707, 1
- Bournaud, F. et al., Chapon, D., Teyssier, R., et al. 2011, *ApJ*, 730, 4
- Brammer, G.B., van Dokkum, P.G. & Coppi, P. 2008, *ApJ*, 686, 1503
- Brammer, G.B., Whitaker, K.E., van Dokkum, P.G., et al. 2011, *ApJ*, 739, 24
- Bruzual, G. & Charlot, S. 2003, *MNRAS*, 344, 1000
- Calzetti, D., Armus, L., Bohlin, R.C., et al. 2000, *ApJ*, 533, 682
- Carilli, C.L., Daddi, E., Riechers, D., et al. 2010, *ApJ*, 714, 1407
- Cassata, P., Giavalisco, M., Guo, Y., et al. 2010, *ApJ*, 714, 79
- Chabrier, G. 2003, *PASP*, 115, 763
- Cimatti, A., Cassata, P., Pozzetti, L., et al. 2008, *A&A*, 482, 21
- Daddi, E., Renzini, A., Pirzkal, N., et al. 2005, *ApJ*, 626, 680
- Daddi, E., Dannerbauer, H., Stern, D., et al. 2009, *ApJ*, 694, 1517
- Emsellem, E., Cappellari, M., Krajnović, D., et al. 2011, *MNRAS*, 414, 888
- Gallazzi, A., Charlot, S., Brinchmann, J., White, S.D.M. 2006, *MNRAS*, 370, 1106
- Gobat, R., Daddi, E., Onodera, M., et al. 2011, *A&A*, 526, 133
- González, V., Labbé, I., Bouwens, R.J., et al. 2010, *ApJ*, 713, 115
- Karim, A., Schinnerer, E., Martínez-Sansigre, A., et al. 2011, *ApJ*, 730, 61
- Kennicutt, R.C. 1998, *ARA&A*36, 189
- Kriek, M., van Dokkum, P.G., Labbé, I., et al. 2009, *ApJ*, 700, 221
- Kümmel, M., Walsh, J.R., Pirzkal, N., Kuntschner, H. & Pasquali, A. 2009, *PASP*121, 59
- Magdis, G.E., Rigopoulou, D., Huang, J.-S. & Fazio, G.G. 2010, *MNRAS*, 401, 1521
- Magdis, G.E., Daddi, E., Béthermin, M., et al. 2012, *arXiv:1210.1035*
- Mancini, C., Daddi, E., Renzini, A., et al. 2010, *MNRAS*, 401, 933
- Maraston, C. 2005, *MNRAS*, 362, 799
- Maraston, C., Daddi, E., Renzini, A., et al. 2006, *ApJ*, 652, 85
- Martig, M., Bournaud, F., Teyssier, R. & Dekel, A. 2009, *ApJ*, 707, 250
- Michałowski, M.J., Watson, D. & Hjorth, J. 2010, *ApJ*, 712, 942
- Navarro, J.F., Frenk, C.S. & White, S.D.M. 1996, *ApJ*, 462, 563
- Onodera, M., Daddi, E., Gobat, R., et al. 2010, *ApJ*, 715, 6
- Onodera, M., Renzini, A., Carollo, M., et al. 2012, *ApJ*, 755, 26
- Peng, C.Y., Ho, L.C., Impey, C.D. & Rix, H.-W. 2010, *AJ*, 139, 2097
- Rodighiero, G., Daddi, E., Baronchelli, I., et al. 2011, *ApJ*, 739, 40
- Salpeter, E.E. 1955, *ApJ*, 121, 161
- Saracco, P., Longhetti, M. & Gargiulo, A. 2011, *MNRAS*, 412, 2707
- Sérsic, J.-L. 1963, *Bol. Assoc. Argentina Astron.*, 6, 41
- Shen, S., Mo, H.J., White, S.D.M., et al. 2003, *MNRAS*, 343, 978
- Springel, V. & Hernquist, L. 2005, *ApJ*, 622, 9
- van Dokkum, P., Franx, M., Kriek, M., et al. 2008, *ApJ*, 677, 5
- Wuyts, S., Labbé, I., Franx, M., et al. 2007, *ApJ*, 655, 51